

Two-band theory of specific heat and thermal conductivity in the mixed state of MgB₂

L. Tewordt and D. Fay

I. Institut für Theoretische Physik, Universität Hamburg, Jungiusstr. 9, 20355 Hamburg, Germany
(May 22, 2019)

We solve the coupled gap equations for the σ - and π -bands of MgB₂ in the vortex state and calculate the resulting field dependencies of the specific heat coefficient γ and the thermal conductivity κ . The crucial parameters of the theory are the interband pairing interaction $\lambda_{\pi\sigma}$ and the ratio $s = \xi_\sigma/\xi_\pi$ of the coherence lengths. For reasonably small $\lambda_{\pi\sigma}$ and s , the small gap Δ_π decreases with increasing magnetic field H much faster than the large gap Δ_σ . This gives rise to the observed rapid increase of γ_π and κ_π for small fields while γ_σ and κ_σ exhibit conventional field dependencies. Inclusion of intraband impurity scattering yields fairly good agreement with experiments for applied fields along the c axis.

Evidence for the existence of two superconducting gaps in MgB₂¹ is provided by the rapid rise of the specific heat coefficient $\gamma_s(H)$ ² and the thermal conductivity $\kappa_s(H)$ ³ at very low fields. These measured field dependencies can be explained qualitatively by assuming two independent bands where the large s-wave pairing gap $\Delta_\sigma \equiv \Delta_1$ is associated with the two-dimensional σ -band and the small s-wave gap $\Delta_\pi \equiv \Delta_2$ is associated with the three-dimensional π -band.⁴ The steep rise of $\gamma_s(H)$ and $\kappa_s(H)$ can be explained qualitatively by assuming that the "virtual" upper critical field for Δ_π is much smaller than that of Δ_σ .² In the present paper we improve the theory of Ref. 4 by taking into account the interband pairing interaction while neglecting the interband impurity scattering.⁵ We first have to solve the two-band gap equations in the presence of the vortex lattices produced by a magnetic field. Generalization of the linearized gap equations near the upper critical field H_{c2} ⁶ to all averaged fields H between H_{c2} and 0 yields, instead of the single gap equation of Ref. 4, the following coupled gap equations for the gaps Δ_i at $T = 0$:

$$\Delta_i = \sum_{j=1}^2 \lambda_{ij} \int_0^{\omega_c} d\omega B_j(\omega, \Delta_j, \Lambda/v_j). \quad (i = 1, 2) \quad (1)$$

Here, the λ_{ij} are the intra- and interband pairing interactions multiplied by the densities of states $N_i(0)$, and the B_j are the spectral functions of the anomalous propagators for the Abrikosov vortex lattice:⁴

$$B_i = \text{Re} \left[\frac{-i\sqrt{\pi} 2 \Delta_{ri} (\Lambda/v_i) w(z_i)}{\{1 + 8\Delta_{ri}^2 (\Lambda/v_i)^2 [1 + i\sqrt{\pi} z_i w(z_i)]\}^{1/2}} \right], \quad (2)$$

$$z_i = 2(\omega + i\gamma_i) \Lambda/v_i; \quad \Lambda = (2eH)^{-1/2}; \quad \gamma_i = \Gamma_i A_i; \quad (3)$$

$$\Delta_{ri} = \Delta_i/D_i; \quad D_i = 1 - 2(\gamma_i \Lambda/v_i) w(z_i). \quad (4)$$

The Γ_i are the normal state impurity scattering rates and the A_i are the field-dependent densities of states. For band 2 (the π -band) we assume a spherical Fermi surface. Then v_2 is replaced by $v_2 \sin \theta$ and B_2 and D_2 are averaged over the polar angle θ with respect to the direction of H . For brevity we omit here, and in the following, the terms containing $\sin \theta$ and the integrations over $d\theta \sin \theta$ from 0 to $\pi/2$. For band 1 (the σ -band) and the field along the c axis, $\theta = \pi/2$ and thus $\sin \theta = 1$.

In the limit $H \rightarrow 0$ the vortex lattice constant $a = (2/\pi)^{1/2} \Lambda$ tends to infinity. Making use of the asymptotic expansion $w(z) \sim i/\sqrt{\pi} z$, the gap equations, Eq.(1), become

$$\Delta_{i0} = \sum_j \lambda_{ij} \int_0^{\omega_c} d\omega \text{Re} \left[\frac{\Delta_{j0}}{(\omega^2 - \Delta_{j0}^2)^{1/2}} \right], \quad (5)$$

where the Δ_{i0} are the gap values at $T = 0$ in zero field. Here we have made use of the relation

$$(\omega + i\gamma_{i0})/\Delta_{ri}^0 = (\omega + i\gamma_{i0}) D_{i0}/\Delta_{i0} = \omega/\Delta_{i0} \quad (6)$$

which can be derived with the help of the expression for D_i in Eq.(4). However, this relation only holds in the absence of interband impurity scattering.⁵

With the help of the Abrikosov parameters, denoted by β_i , we now express Λ/v_i in terms of the reduced field $h = H/H_{c2}$ and the zero-field gap Δ_{i0} :⁴

$$\Lambda/v_1 = (6\beta_1 h \Delta_{10}^2)^{-1/2}; \quad \Lambda/v_2 = s (6\beta_2 h \Delta_{20}^2)^{-1/2}; \quad s = (v_1/v_2)(\Delta_{20}/\Delta_{10}) = \xi_{10}/\xi_{20}. \quad (7)$$

Employing these relations we can express the gaps Δ_i and the scattering rates Γ_i in Eq.(2) by their ratios with respect to the Δ_{i0} , and we can convert the integrations over ω in Eq.(1) to integrations over the new variables $\Omega = \omega/\Delta_{i0}$. We then divide Eq.(1) by Δ_i and Eq.(5) by Δ_{i0} and subtract the latter from the former. In this way we obtain two coupled equations for the two unknown functions $x_1(h)$ and $x_2(h)$ for given values of the parameters λ_{ij} , δ_i , β_i , r , and s . The quantities x_i , δ_i , and r are defined by

$$x_i = \Delta_i/\Delta_{i0}; \quad \delta_i = \Gamma_i/\Delta_{i0}; \quad r = \Delta_{20}/\Delta_{10}. \quad (8)$$

In Fig. (1) we show the reduced gap functions $x_1(h)$ and $x_2(h)$ for parameter values $\lambda_{11} = 1$, $\lambda_{22} = 0.3$, $\lambda_{12} = 0.1$, $\lambda_{21} = 0.03$, $\delta_1 = 0.5$, $\delta_2 = 0.8$, $r = 1/3$, $1/4$, and $1/5$, with $s = 1/3$, $1/4$, and $1/5$. These values for λ_{11} , λ_{22} , and λ_{12} agree approximately with the values obtained from band structure calculations.⁷ We have, however, taken a much smaller λ_{21} than the value of $\lambda_{\pi\sigma} = 0.091$ given in Ref. 7. The reduced impurity scattering rates δ_i and the values for the ratios r and s agree qualitatively with the values estimated from experiments on MgB₂. While the function $x_1(h) \simeq (1 - h)^{1/2}$ is rather independent of the choice of parameters, the function $x_2(h)$ depends sensitively on the value of the coupling constant λ_{21} . As λ_{21} tends to the theoretical value of 0.091 of Ref. 7, $x_2(h)$ is rather close to $x_1(h)$ and consequently the functions $\gamma_s(H)$ and $\kappa_s(H)$ for the two bands are not very different. For vanishing interband coupling λ_{21} , however, we obtain approximately $x_2(h) \simeq (1 - h/s^2)^{1/2}$ which goes to zero at a smaller effective upper critical field $H_{c2}^\pi = s^2 H_{c2}$ where $s \simeq \xi_{10}/\xi_{20}$ (see Eq.(7)). Thus we see that H_{c2}^π corresponds to the "virtual" upper critical field for the π -band which was introduced in Ref. 2 as the field above which the overlap of the vortex cores with large radius ξ_{20} (see the STS measurements of Ref. 8) drives the majority of the π -band electrons normal. In Fig.(1) we show $x_i(h)$ for $s = r = 1/3$ and for the smaller values $s = 1/4$ and $1/5$ which take into account that, in Eq.(7), $v_1/v_2 < 1$.⁹ The gap $x_2(h)$ is seen to decrease more rapidly relative to $x_1(h)$ as s is decreased, remaining, however, finite up to $h = 1$.

In Fig.(2) we have plotted our results for the zero energy density of states $A_i(\omega = 0)$ obtained from the expression for A_i (given by Eq.(2) with the numerator set equal to 1) by inserting the previously calculated gap ratios $x_i(h)$ together with Eqs.(7) for the functions $\Lambda(h)/v_i$. A_2 is obtained by averaging $A_2(\theta)$ over the polar angle θ . We note that it is important to calculate the impurity scattering rates $\gamma_i = \Gamma_i A_i(h)$ self-consistently. One sees from Fig. (2) that $A_2(h)$ rises steeply for small fields h and then becomes almost constant above $h \sim 0.2$. The slope at $h = 0$ and the downward curvature for low fields increase as s is decreased from $1/3$ to $1/4$ to $1/5$. The function $A_1(h)$ is very similar to the function obtained previously for a single band.⁴ The initial steep rise of $A_2(h)$ qualitatively fits the data points for the contribution of the π -band to the specific heat coefficient $\gamma(H)$.² The function $A_1(h)$ corresponds to the straight line assumed in Ref. 2 for the σ -band contribution to $\gamma(H)$ for fields applied along the c axis.

We turn now to the calculation of the in-plane electronic thermal conductivity $\kappa_s(h)$ which is given at $T = 0$ by the expression in Ref. 10. Again it is important to take into account the renormalization of the gap by the function D_i in the presence of impurity scattering (see Eq.(13) of Ref. 4). By inserting the functions $x_i(h)$ obtained from the gap equations, Eq.(1), and the functions $\Lambda(h)/v_i$ from Eq.(7) into the expressions for the ratios κ_s/κ_n we obtain, for applied fields \mathbf{H} along the c axis, the thermal conductivity ratios $\kappa_{si}(h)/\kappa_{ni}$ shown in Fig.3. It should be noted that the π -band contribution $\kappa_{s2}(h)/\kappa_{n2}$ has been obtained as an average over the polar angle θ by including the factor $(3/2) \sin^2 \theta$ which arises from the square of the group velocity in the ab plane. The curve for the σ -band conductivity $\kappa_{s1}(h)/\kappa_{n1}$ turns out to be very similar to the curve obtained in Ref. 4 for a single band with the same impurity scattering rate $\delta_1 = 0.5$. The curve $\kappa_{s2}(h)/\kappa_{n2}$ for the π -band contribution with $\delta_2 = 0.8$ rises almost linearly with h where the slope near $h = 0$ and the downward curvature for low fields increase as s is decreased from $1/3$ to $1/4$ to $1/5$. For applied fields perpendicular to the c axis, the measured thermal conductivity κ_e first rises steeply for small fields and then saturates while, for fields along the c axis, it exhibits an upward curvature towards H_{c2} .³ These different behaviors have been explained by separating the individual contributions of the π - and σ -bands. Then κ_π rises steeply with H and approximately attains its normal-state value at a small field and κ_σ first rises very slowly and then curves upward towards H_{c2} .³ These experimental curves are similar to our results for $s = 1/4$ shown in Fig. (3).

We now briefly discuss the parameter values and approximations that have been used to derive our results. We have seen that the rapid increase of the specific heat coefficient $\gamma_s(h)/\gamma_n$ and the thermal conductivity ratio $\kappa_s(h)/\kappa_n$ with increasing field $h = H/H_{c2}$ is due mainly to the π -band contribution. The reason is that the gap $\Delta_2(h)$ associated with the π -band almost closes at the so-called "virtual" upper critical field² $H_{c2}^\pi \sim s^2 H_{c2}$ because the ratio $s = \xi_{10}/\xi_{20}$

of the coherence lengths of the σ - and the π -bands is much smaller than 1. For the most important parameters entering our gap equations, s and $r = \Delta_{20}/\Delta_{10}$, we have used the values $r = 1/3$ and $s = 1/3, 1/4$, and $1/5$ which are based on various experiments on MgB₂.^{2,8,9} The field dependence of the gap ratio $x_1(h) = \Delta_1/\Delta_{10}$, and thus of the contributions to γ_{s1}/γ_{n1} and κ_{s1}/κ_{n1} arising from the σ -band, are nearly the same as those obtained for an independent single σ -band,⁴ indicating that the effect of the interband coupling $\lambda_{12} \sim 0.1$ is rather small. However, the field dependence of $x_2(h) = \Delta_2/\Delta_{20}$ differs substantially from that for the independent single π -band with an effective upper critical field $h_{c2}^\pi = s^2$ as can be seen from Fig.(1). This is because $x_2(h)$ is non-zero between h_{c2}^π and $h = 1$ due to the effect of the interband coupling λ_{21} . This shows that superconductivity survives even though the vortex cores for the π -band with giant radius ξ_{20} ⁸ start to overlap for $h > h_{c2}^\pi$. As can be seen in Fig.(1), the curve for $x_2(h)$ is very sensitive to the values of λ_{21} and s . We find that the experimental contributions to γ and κ arising from the π -band^{2,3} can only be fitted by assuming rather small values of $\lambda_{21} \simeq 0.03$, while band structure calculations yield a much larger value, $\lambda_{21} \simeq 0.09$.⁷ The other crucial parameter value needed to obtain good fits of the data is $s \simeq 1/4$. Taking a smaller value than $s = r = 1/3$ is reasonable since the ratio of velocities v_1/v_2 in Eq.(7) is smaller than 1.⁹ The other parameter values used in our numerical calculations are the reduced impurity scattering rates $\delta_1 = 0.5$ and $\delta_2 = 0.8$ which have been estimated from the relevant experiments. It turns out that even for these moderately large impurity scattering rates it is very important to take into account the renormalization of the gap (see Eq.(4)) which leads to a large reduction of the effect of impurity scattering in comparison to that calculated without the function D . It is also important that the calculation of the scattering rate $\gamma_i = \Gamma_i A_i(h)$ in the Born limit be carried out self-consistently together with the calculation of the zero-energy density of states $A_i(h)$. This yields $A_i(0) = 0$, as it should. The shape of the Fermi surface (FS) and the direction of the applied field play an important role because the spectral functions B_i in Eq.(2) have to be averaged over the corresponding FS where the velocity v_i denotes the component $v_{i\perp}(\mathbf{p})$ perpendicular to \mathbf{H} . For the spherical FS we have assumed for the π -band, $v_{\perp}(\mathbf{p}) = \mathbf{v} \sin \theta$, where $\theta = \angle(\mathbf{p}, \mathbf{H})$. In the limit $\theta \rightarrow 0$ the function B approaches the BCS spectral function of the anomalous propagator. We find that the results for the averages over the polar angle θ do not differ significantly from the results obtained by setting $\theta = \pi/2$. This means that the quasiparticles moving perpendicular to the vortex axes yield the dominant contributions to γ and κ . Finally it should be pointed out that we have employed the Abrikosov ground state of the vortex lattice although, in particular at lower fields, a Landau-level expansion or a variational expression⁶ is needed to describe the distorted vortex lattice. The results for $\gamma_s(h)/\gamma_n$ and $\kappa_s(h)/\kappa_n$ shown in Figs.(2) and (3) for the σ - and π -bands should still be added by weighting them with the corresponding density of states. One sees that qualitative fits of the measured field dependencies of the specific heat² and the thermal conductivity³ for applied fields along the c axis can be obtained by adjusting the crucial parameters λ_{21} for the interband pairing interaction and the ratio $s = \xi_{10}/\xi_{20}$ of the coherence lengths.

In conclusion we can say that our two-band theory for the vortex state in MgB₂ can satisfactorily account for the observed field dependence of the specific heat coefficient γ and the thermal conductivity κ . The small gap Δ_2 associated with the π -band decreases with increasing field H much faster than the large σ -band gap Δ_1 which shows conventional field dependence. This gives rise to the rapid increase of γ and κ at small fields. Due to a small interband pairing interaction λ_{21} , the gap Δ_2 remains finite even in the field region where the large π -band vortex cores of radius ξ_{20} overlap. This leads to smooth evolution of the π -band contributions to γ and κ to their normal state values near a "virtual" upper critical field $H_{c2}^\pi \simeq s^2 H_{c2}$ which is much smaller than H_{c2} because the ratio $s = \xi_{10}/\xi_{20}$ is much smaller than 1. The Fermi surface topology and the impurity scattering have relatively small influence on the field dependence of γ and κ for fields applied along the c axis.

We would like to thank T. Dahm and K. Scharnberg for valuable discussions.

¹ J. Nagamatsu, N. Nakagawa, T. Muranaka, Y. Zenitani, and J. Akimitsu, *Nature* **410**, 63 (2001).

² F. Bouquet, Y. Wang, I. Sheikin, T. Plackowski, A. Junod, S. Lee, and S. Tajima, *Phys. Rev. Lett.* **89**, 257001-1 (2002).

³ A. V. Sologubenko, J. Jun, S. M. Kazakov, J. Karpinski, and H. R. Ott, *Phys. Rev. B* **66**, 014504 (2002).

⁴ L. Tewordt and D. Fay, *Phys. Rev. B* (in press).

⁵ N. Schopohl and K. Scharnberg, *Solid State Commun.* **22**, 371 (1977).

⁶ T. Dahm and N. Schopohl, *cond-mat/0212188*.

⁷ A. Y. Liu, I. I. Mazin, and J. Kortus, *Phys. Rev. Lett.* **87**, 087005 (2001).

⁸ M. R. Eskildsen, M. Kugler, S. Tanaka, J. Jun, S. M. Kazakov, J. Karpinski, and Ø. Fischer, *Phys. Rev. Lett.* **89**, 187003-1 (2002).

⁹ A. Brinkman et al, *Phys. Rev. B* **65**, 180517(R) (2002).

¹⁰ L. Tewordt and D. Fay, *Phys. Rev. B* **64**, 24528 (2001).

Fig. 1

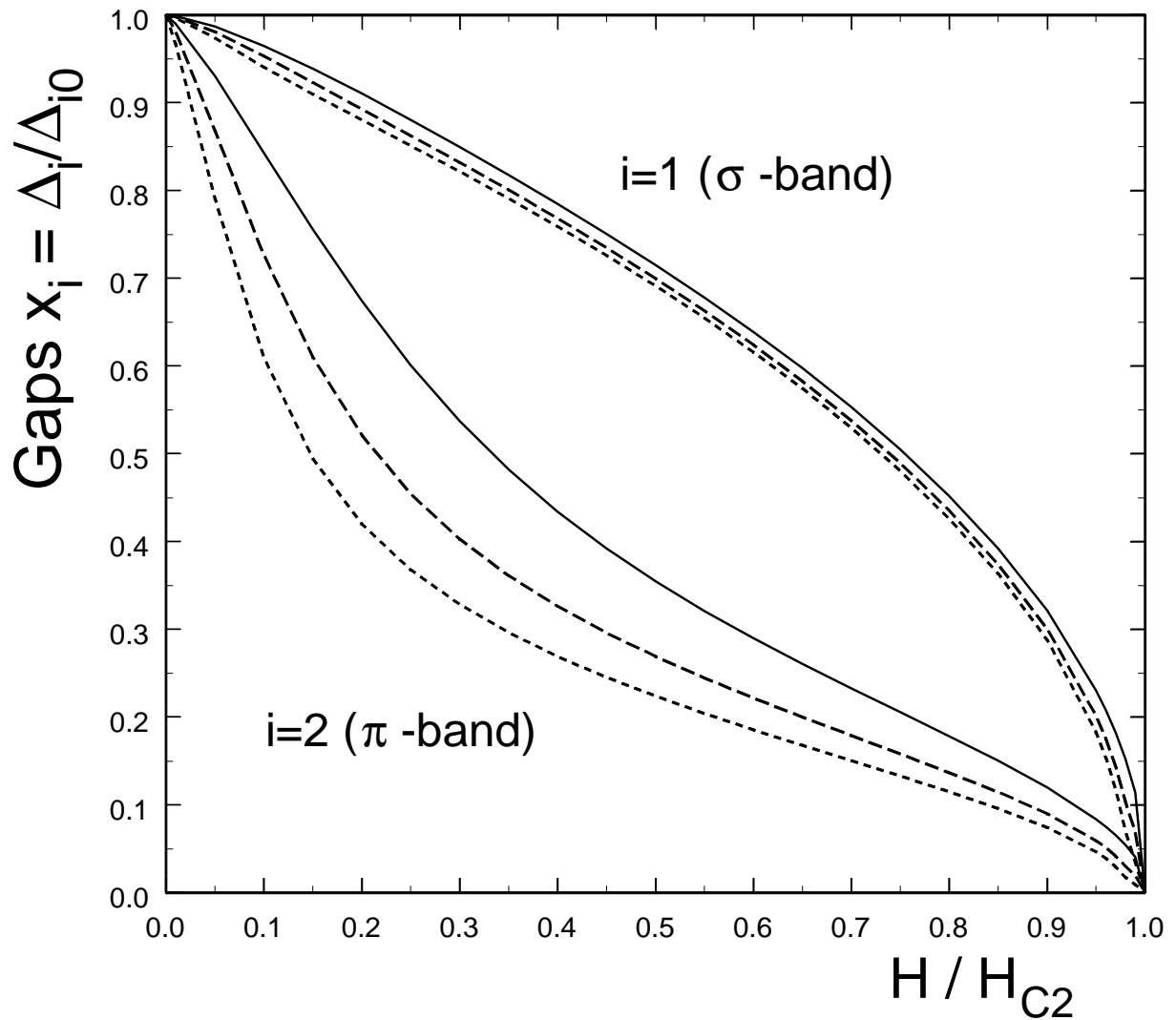


FIG. 1. Reduced gaps $x_1(h) = \Delta_1/\Delta_{10}$ for the σ -band and $x_2(h) = \Delta_2/\Delta_{20}$ for the π -band vs reduced magnetic field $h = H/H_{c2}$ for applied fields along the c axis. The upper curves are for x_1 and the lower curves for x_2 . The interband pairing interaction λ_{21} has the value 0.03 and the ratio of coherence lengths is $s = \xi_{10}/\xi_{20} = 1/3, 1/4$, and $1/5$, from top to bottom. The reduced impurity scattering rates δ_i and Abrikosov parameters β_i are $\delta_1 = 0.5$ and $\beta_1 = 1.3$ for the σ -band and $\delta_2 = 0.8$ and $\beta_2 = 1.58$ for the π -band.

Fig. 2

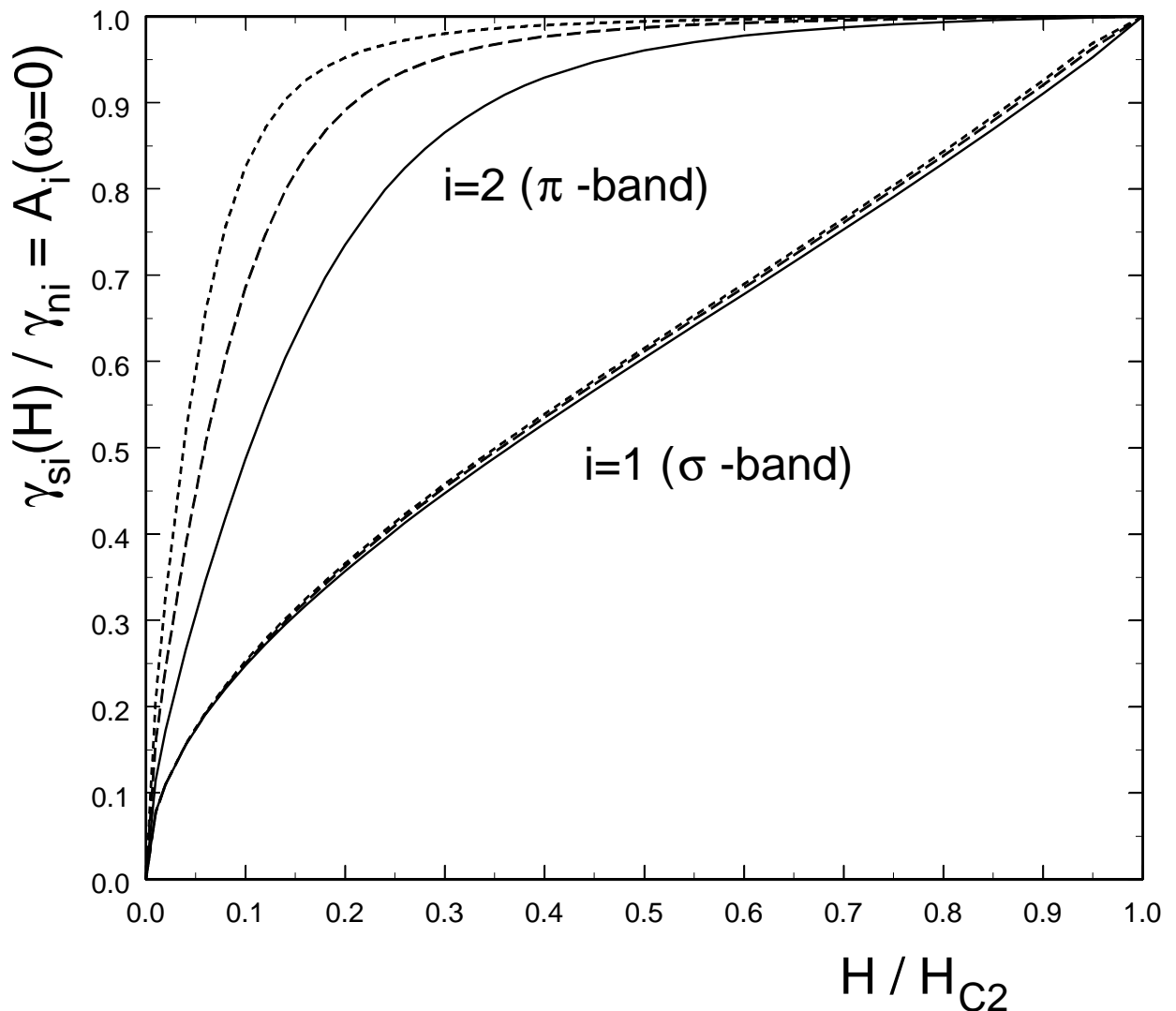


FIG. 2. Specific heat coefficients, or zero-energy densities of states, $\gamma_{si}/\gamma_{ni} = A_i$, ($i = 1, 2$) vs h for the parameter values of Fig.(1). The lower curves are for the σ -band, $i = 1$, and the upper curves are for the π -band, $i = 2$, with the ratio of coherence lengths $s = \xi_{10}/\xi_{20} = 1/3, 1/4$, and $1/5$, from bottom to top.

Fig. 3

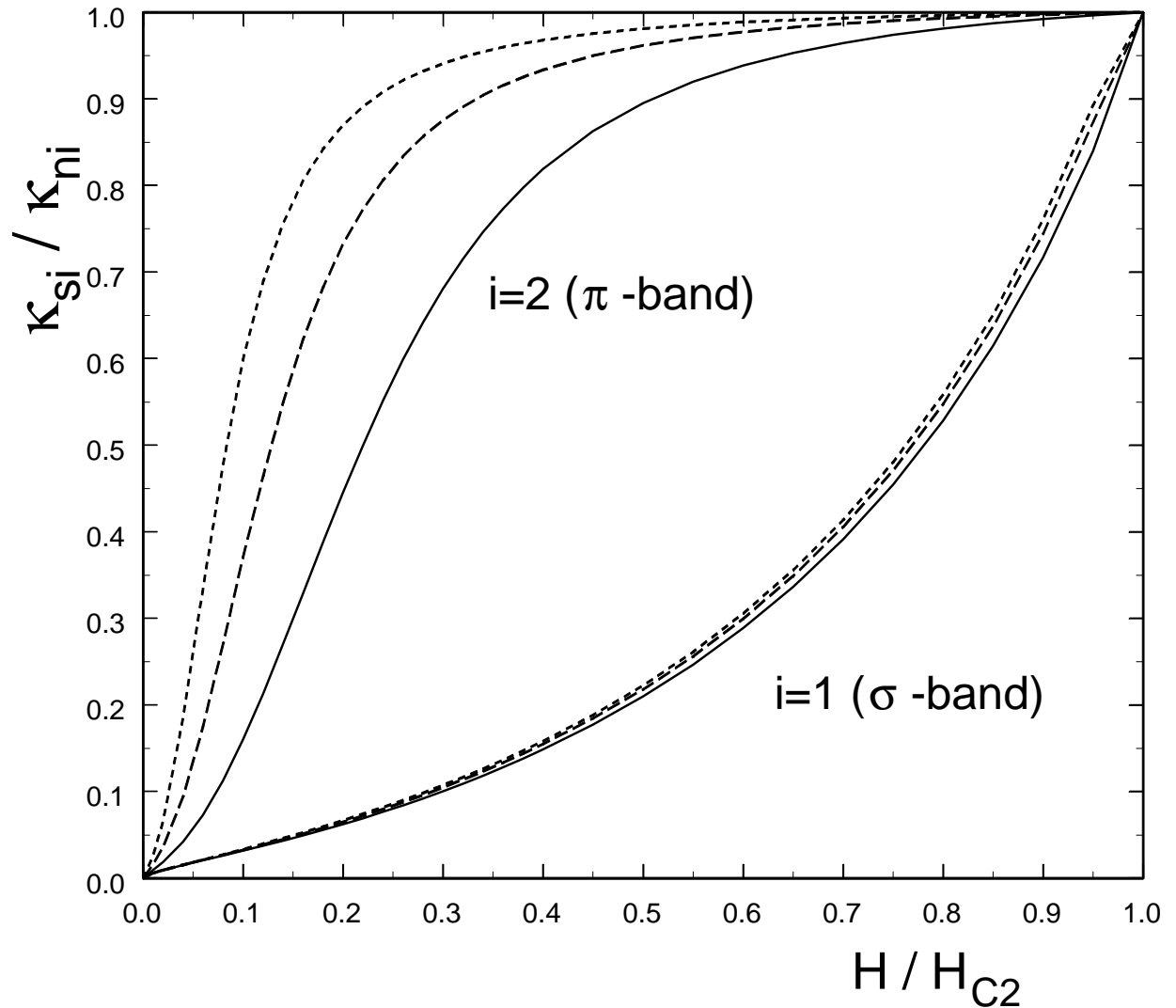


FIG. 3. Reduced electronic thermal conductivities, κ_{si}/κ_{ni} , ($i = 1, 2$) vs h for the parameter values of Fig.(1). The lower curves are for the σ -band, $i = 1$, and the upper curves are for the π -band, $i = 2$, with the ratio of coherence lengths $s = \xi_{10}/\xi_{20} = 1/3, 1/4$, and $1/5$, from bottom to top.